PHYSICAL REVIEW B **94**, 241104(R) (2016)

Absence of full many-body localization in the disordered Hubbard chain

P. Prelovšek,[1,2] O. S. Barišić,[3] and M. Žnidarič[2]
[1]*Jožef Stefan Institute, SI-1000 Ljubljana, Slovenia*
[2]*Faculty of Mathematics and Physics, University of Ljubljana, SI-1000 Ljubljana, Slovenia*
[3]*Institute of Physics, HR-1000 Zagreb, Croatia*

(Received 12 October 2016; revised manuscript received 29 November 2016; published 12 December 2016)

We present numerical results within the one-dimensional disordered Hubbard model for several characteristic indicators of the many-body localization (MBL). Considering traditionally studied charge disorder (i.e., the same disorder strength for both spin orientations) we find that even at strong disorder all signatures consistently show that while charge degree of freedom is nonergodic, the spin is delocalized and ergodic. This indicates the absence of the full MBL in the model that has been simulated in recent cold-atom experiments. Full localization can be restored if spin-dependent disorder is used instead.

DOI: 10.1103/PhysRevB.94.241104

Introduction. The many-body localization (MBL) is a phenomenon whereby an interacting many-body system localizes due to disorder, proposed [1,2] in analogy to the Anderson localization of noninteracting particles [3,4]. The MBL physics has attracted a great deal of attention from theoreticians. Yet, it has so far been predominantly studied within the prototype model, i.e., the one-dimensional (1D) model of interacting spinless fermions with random potentials, equivalent to the anisotropic spin-1/2 Heisenberg chain with random local fields. Emerging from these studies are the main hallmarks of the MBL state of the system: (a) the Poisson many-body level statistics [5–9], in contrast to the Wigner-Dyson one for normal ergodic systems; (b) vanishing of dc transport at finite temperatures $T > 0$, including the $T \to \infty$ limit [10–17]; (c) logarithmic growth of the entanglement entropy [18–20], as opposed to linear growth in generic systems; (d) an existence of a set of local integrals of motion [21–24]; and (e) a nonergodic time evolution of (all) correlation functions and of quenched initial states [25–29]. Because of these unique properties, the MBL can be used, e.g., to protect quantum information [30,31]. For more detailed review, see Refs. [32,33].

The experimental evidence for the MBL comes from recent experiments on cold atoms in optical lattices [34–37] and ion traps [38]. In particular, for strong disorders, experiments reveal nonergodic decay of the initial density profile in uncoupled [34] and coupled [36] 1D fermionic chains, as well as the vanishing of dc mobility in a three-dimensional disordered lattice [35]. In contrast to most numerical studies, being based on the spinless fermion models, the cold-atom experiments simulate a disordered Hubbard model. The latter has been much less investigated theoretically [34,39,40], whereby results show that density imbalance might be nonergodic at strong disorder [34,39], in accordance with experiments [34,36].

The essential difference with respect to the interacting spinless model is that the Hubbard model has two local degrees of freedom: charge (density) and spin. The aim of this Rapid Communication is to present numerical evidence that in the case of a (charge) potential disorder and finite repulsion $U > 0$ (as, e.g., realized in the cold-atom experiments), both degrees behave qualitatively differently. In particular, while for strong disorder the charge exhibits nonergodic behavior (e.g., the charge-density-wave and the local charge correlations fail to reach the thermal equilibrium), the spin imbalance and the local spin correlations show a clear decay. Similarly, we find that dc charge conductivity vanishes with the increasing disorder, whereas spin conductivity remains finite in the dc limit or is at least subdiffusive. The entanglement entropy, which incorporates both degrees, grows as a power law with time. All these findings reveal that even for strong disorders the system does not follow the full MBL scenario, requiring the existence of a full set of local conserved quantities [21,22,32]. The present results point towards a phenomenon of a partial nonergodicity and an effective dynamical charge-spin separation. Furthermore, we show that the localization of the spin degree of freedom may be achieved when the symmetry between the up and down fermions is lifted, for instance, by introducing a spin-dependent disorder.

Model. The 1D disordered Hubbard model is given by the Hamiltonian,

$$H = -t_0 \sum_{js} (c^{\dagger}_{j+1,s} c_{js} + \text{H.c.}) + U \sum_j n_{j\uparrow} n_{j\downarrow} + \sum_j \epsilon_j n_j, \tag{1}$$

where $n_j = n_{j\uparrow} + n_{j\downarrow}$ is the local (charge) density. In our analysis, we consider the local (spin) magnetization as well, given by $m_j = n_{j\uparrow} - n_{j\downarrow}$. The quenched local potential disorder in Eq. (1) involves a random uniform distribution $-W < \epsilon_j < W$. $t_0 = 1$ is used as the unit of energy. In order to look for possible MBL features of the whole many-body spectrum, we focus our numerical calculations on the $T \to \infty$ limit. With the average density $\bar{n} = \frac{1}{L}\sum_j n_j$ and the average magnetization $\bar{m} = \frac{1}{L}\sum_j m_j$ being constants of motion, we choose to investigate the unpolarized system $\bar{m} = 0$ and the half-filling $\bar{n} = 1$ case, which is a generic choice at high T. Nevertheless, we also test the quarter-filling case, $\bar{n} = 1/2$ (see the Supplemental Material [41]), as it is the one realized in experiments [34,36].

Imbalance correlations. In connection with cold-atom experiments are most relevant charge (density) imbalance correlations $I(t)$ as they evolve in time from an initial out-of-equilibrium configuration. Therefore, we first discuss related charge-density-wave (CDW) and spin-density-wave (SDW)

autocorrelation functions,

$$C(\omega) = \frac{\alpha}{L}\mathrm{Re}\int_0^\infty dt\, e^{i\omega t}\langle n_\pi(t) n_\pi\rangle,$$
$$S(\omega) = \frac{\alpha}{L}\mathrm{Re}\int_0^\infty dt\, e^{i\omega t}\langle m_\pi(t) m_\pi\rangle, \qquad (2)$$

calculated for a particular (staggered) wave vector $q = \pi$, with $n_{q=\pi} = \sum_j (-1)^j n_j$ for the CDW case, and $m_{q=\pi} = \sum_j (-1)^j m_j$ for the SDW case. In Eq. (2), $1/\alpha = \bar{n}(1 - \bar{n}/2)$ so that $C(t=0) = S(t=0) = 1$, for $T, L \to \infty$. The nonergodicity (after taking $L \to \infty$) should manifest itself as a singular contribution, $C(\omega \sim 0) = C_0\delta(\omega)$, $S(\omega \sim 0) = S_0\delta(\omega)$, with C_0 and S_0 corresponding to the CDW and the SDW stiffnesses, respectively. That is, the (full) MBL requires that both C_0 and S_0 are finite. For the calculation of imbalance correlations we employ the microcanonical Lanczos method (MCLM) [42,43] on finite systems of maximum length $L = 14$ for $\bar{n} = 1$ (for $\bar{n} = 1/2$ see the Supplemental Material [41]). The high frequency resolution is achieved by a large number of Lanczos steps $N_L = 10^4$, $\delta\omega \propto 1/N_L$. The averaging over disorder realizations is performed over $N_s = 20$–100 different ϵ_j configurations.

Instead of plotting spectra $C(\omega), S(\omega)$, given by Eq. (2), it is more informative to display quasi-time-evolution $C, S(\tau) = \int_{-1/\tau}^{1/\tau} d\omega C, S(\omega)$. In this way we omit fast oscillations with typical $\omega = t_0$, while retaining the physical content of the limit $t = \tau \to \infty$. In Fig. 1 we compare results for $C(\tau)$ and $S(\tau)$ at half-filling $\bar{n} = 1$ for intermediate $U = 4$ and a wide span of disorder $W = 2$–15, obtained by the MCLM for $L = 14$. (In the Supplemental Material [41] we compare results obtained for different L, showing that they are mutually consistent for $L \geqslant 10$.) Results are plotted up to maximum times $\tau_m = 1/\delta\omega$, where for different $L \leqslant 14$ we get $\tau_m = 50$–200, depending on W.

The results presented in Fig. 1 reveal a qualitative difference between charge and spin dynamics within the Hubbard model. For $C(\tau)$ we observe a behavior that is qualitatively very similar to the behavior of the density imbalance in the spinless model [7,28], or to the behavior reported in experiments [34,36]. Namely, in the presence of finite $U > 0$, the CDW correlations are ergodic $C(\tau \to \infty) \to 0$ for weak disorders $W = 2,3$, while for large disorders, e.g., $W = 6,15$, the nonergodicity appears, $C(\tau \to \infty) = C_0 > 0$. This is in clear contrast with the spin imbalance case, $S(\tau)$, which decays to zero even for the strongest disorder $W = 15$. Although the ergodic-nonergodic transition from CDW correlations in Fig. 1 cannot be precisely located, $W^* \sim 4$–6, it is clearly there. On the other hand, no such transition can be observed in SDW correlations, which remain ergodic independently of disorder strength.

A similar message is obtained from $C, S(\tau)$, being presented in Fig. 2 for fixed W as a function of interaction U. In Fig. 2, the disorder strength is set to $W = 6$, because for $U = 4$ such W corresponds to the nonergodic regime for CDW correlations, as shown in Fig. 1. The noninteracting $U = 0$ case is a particular one, involving the Anderson localization of single-particle states. Consequently, for $U = 0$ both $C(\tau)$ and $S(\tau)$ in Fig. 2 saturate to a constant value after a short transient $\tau \sim 1$. For $U > 0$, the behavior of $C(\tau)$ and $S(\tau)$ turns out to be very different. $C(\tau)$ exhibits a weak variation with $U > 0$, but still with weak logarithmiclike time dependence [28]. On the other hand, already the $U = 1$ case leads to a decay of spin imbalance $S(\tau \to \infty) = 0$. This decay becomes even faster for $U = 4,8$.

Local correlations. Next we study local charge and spin dynamics, by considering the local real-time correlation $C_l(t) = A\sum_j \langle \rho_j(t)\rho_j\rangle$ and $S_l(t) = B\sum_j \langle m_j(t) m_j\rangle$, where $\rho_j = n_j - \bar{n}$, while A and B are normalization constants such that $C_l(0) = S_l(0) = 1$. Similarly as for the imbalance, in a MBL system these two quantities freeze at a nonzero value [27], indicating the nonergodicity. The advantage of the

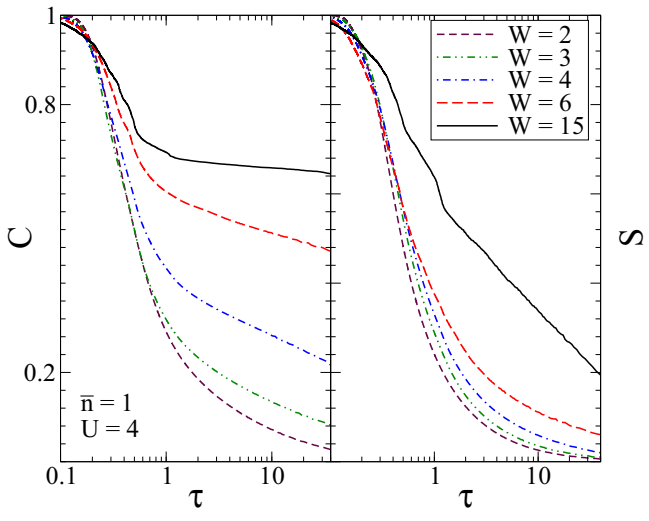

FIG. 1. Charge and spin imbalance correlations $C(\tau)$ and $S(\tau)$, respectively, as evaluated by the MCLM at half-filling $\bar{n} = 1$ and $U = 4$, at fixed system size $L = 14$. The potential disorder is varied in the range $W = 2$–15.

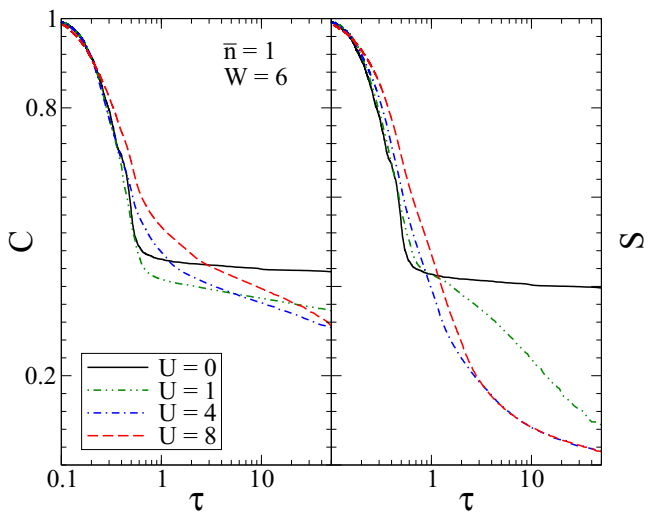

FIG. 2. $C(\tau)$ and $S(\tau)$ calculated for half-filling $\bar{n} = 1$ and $L = 12$, for fixed disorder $W = 6$ and various interaction strengths $U = 0$–8.

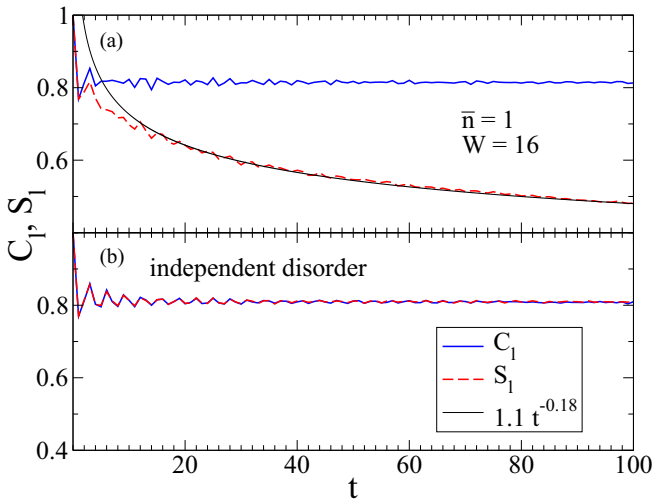

FIG. 3. Decay of the local charge and spin correlations for $U = 1$ and $W = 16$. (a) For the charge disorder, spin is delocalized (the red dashed curve). (b) For the independent disorder for each spin, the charge and the spin are both localized (note the two, the red and the blue curves, almost completely overlapping). The averaging involves over 400 product initial states, $L = 64$.

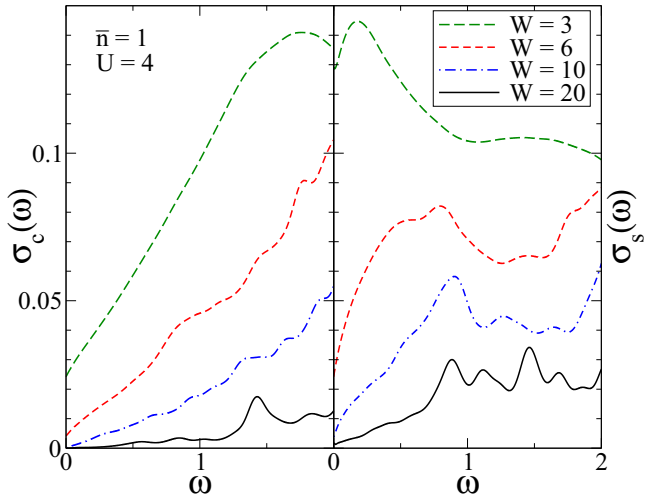

FIG. 4. Charge and spin dynamical conductivity $\sigma_c(\omega)$ and $\sigma_s(\omega)$, respectively, evaluated at half-filling $\bar{n} = 1$, $U = 4$ at fixed size $L = 14$, but for various disorders $W = 3$–20.

autocorrelation functions C_l and S_l over imbalance is that they exhibit smaller fluctuations for generic initial states.

For the current analysis of the local correlations (as well as for calculations of the entropy afterwards), we use the time-dependent density matrix renormalization group method, which is an efficient method for evolution of initial product states provided the entanglement is small. For strong disorder we are typically able to simulate significantly larger systems ($L \approx 64$) than with the MCLM. Details of the method as well as references to original literature may be found in, e.g., Ref. [18]. In Fig. 3 we show the results of such a simulation. One may see that even for very strong disorders W and small interactions U the spin autocorrelation function decays algebraically (unlike charge), again signaling the ergodicity of the spin degree of freedom.

On the other hand, by considering a modification of the disorder model in Eq. (1) and taking an independent disorder for the each spin orientation, i.e., $\sum_j (p_j n_{j\uparrow} + q_j n_{j\downarrow})$ with independent p_j and $q_j \in [-W, W]$, a dramatic change occurs. As may be seen from Fig. 3(b), now both the spin and the charge behave in the same way, freezing at a nonzero value, as expected for the MBL system.

Dynamical conductivities. The question of dc transport is frequently analyzed in the context of dynamical charge and spin conductivities (or diffusivities, since we omit the prefactor $1/T$). In the $T \to \infty$ limit, these two conductivities are given by

$$\sigma_{c,s}(\omega) = \frac{1}{L} \mathrm{Re} \int_0^\infty dt\, e^{i\omega t} \langle j_{c,s}(t) j_{c,s} \rangle, \tag{3}$$

where $j_{c,s}$ are charge and spin uniform currents, respectively, $j_{c,s} = i \sum_{is} (\pm 1)^s (c^\dagger_{i+1,s} c_{is} - c^\dagger_{is} c_{i+i,s})$.

For the evaluation of $\sigma_{c,s}(\omega)$ we again employ the MCLM, using periodic boundary conditions. The numerical requirements are similar as for $C, S(\omega)$. Namely, the crucial role is played again by the high ω resolution, because the quantities of interest here are the dc value $\sigma_{c,s}(\omega \to 0)$ and the low-ω scaling of $\sigma_{c,s}(\omega) - \sigma_{c,s}(0)$ with ω.

Results for $\sigma_c(\omega)$,$\sigma_s(\omega)$ are presented in Fig. 4, for intermediate $U = 4$ and a wide range of disorders, $W = 3$–20. It should be pointed out that due to insufficient sampling, N_s, the current results for strongest $W > 10$ suffer in part from sample-to-sample fluctuations, which increase with W. On the other hand, the results for weaker W are much less sensitive to fluctuations [16]. Conclusions that follow from $\sigma_c(\omega)$ in Fig. 4 are quite similar to those obtained for the spinless model [11,15,16,44]. The maximum of $\sigma_c(\omega)$ at moderate disorder $W \geqslant 2$ is at $\omega_c^* \sim 2$, reflecting the noninteracting limit. At low $\omega \ll 1$, we find rather generic nonanalytical behavior $\sigma_c(\omega) \sim \sigma_c(0) + \zeta |\omega|^\alpha$ with $\alpha \sim 1$. dc value $\sigma_s(0)$ is rapidly vanishing for $W > 4$.

On the other hand, in Fig. 4, $\sigma_s(\omega)$ behaves qualitatively differently. In general, it exhibits two maxima, whereby the lower one at $\omega_s^* < 1$ is not present in $\sigma_c(\omega)$, indicating a different scale for the spin dynamics. In addition, finite $\sigma_s(0) > 0$ seems to be well resolved all the way up to $W = 20$. Moreover, the low-ω behavior appears to be given by $\sigma_s(\omega) \sim \sigma_s(0) + \xi |\omega|^\gamma$, with $\gamma < 1$ even for the largest W. The implication of $\gamma < 1$, being an indication of a subdiffusive dynamics [12,45], is divergent static magnetic polarizability $\chi_s \propto \int d\omega\, \sigma_s(\omega)/\omega^2$, even in the case of vanishing dc $\sigma_s(0) = 0$. This low-frequency behavior of $\sigma_s(\omega)$ is compatible with a subdiffusive spin transport $\Delta m \sim t^{0.3}$, observed for initial states with global spin imbalance (see the Supplemental Material [41] for details). Thus, spin (magnetization) is transported globally even for strong disorder.

Entanglement entropy. One of the defining properties of the MBL is logarithmic growth of entanglement with time [18], when starting from a product initial state. In Fig. 5 the behavior of the entanglement entropy $S_2(t) = -\mathrm{tr}[\rho_A(t) \log_2 \rho_A(t)]$ of the reduced density matrix $\rho_A(t)$ is shown for $U = 1$ and large W. From the semilogarithmic plot (the inset in Fig. 5) one may see that $S_2(t)$ has a slight upward curvature, not growing

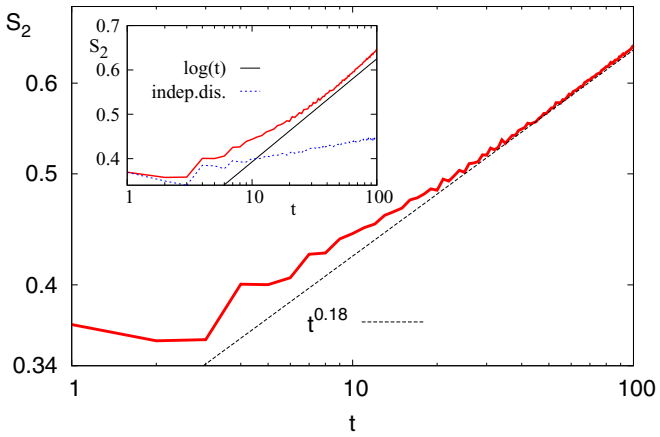

FIG. 5. Average von Neumann entropy $S_2(t)$ for $U = 1$ and $W = 16$ in a log-log plot. Inset: semilogarithmic plot of the same data (red curve). For charge disorder (red curve) $S_2(t)$ is consistent with a power law, while for an independent disorder (blue curve in the inset) with a logarithmic growth. The same dataset as in Fig. 3, statistical fluctuations are of the size of curves thickness.

logarithmically. Indeed, as shown in main frame, the growth is better described by a power law, $S_2(t) \sim t^{0.18}$ [the power ≈ 0.18 seems to be the same as the power of the decay of $S_l(t)$ in Fig. 3]. On the other hand, with the independent disorder $W = 16$ on both spin orientations one gets $S_2(t) \sim \log(t)$ (the blue curve in the inset in Fig. 5).

Symmetry argument. The ergodicity of the spin degrees has been so far established numerically. However, we wish to present additional symmetry arguments for $\bar{n} = 1$ and $\bar{m} = 0$ to demonstrate that $S_l(t \to \infty) \to 0$ for any fixed L. That is, in the absence of degeneracy, $S_l(t \to \infty)$ in the eigenbasis of H is given solely by diagonal matrix elements of m_j. For charge disorder, H is even under operation P that exchanges up and down fermions. Consequently, all eigenstates for $U \neq 0$ have a well defined parity P, while m_j is odd under P, and therefore all diagonal matrix elements of m_j are zero by symmetry. The order of limits $L \to \infty, t \to \infty$ used above is opposite to the one required for a proof of ergodicity. Namely, there is always a possibility for the existence of an intermediate "freezing" time scale $t_f(L)$ at which $S_l(t_f) > 0$, with $t_f(L)$ diverging in the thermodynamic $L \to \infty$ limit. However, our numerical data (see also Ref. [41]) does not give any hints for such behavior of $t_f(L)$.

Conclusions. We have presented numerical results for the 1D Hubbard model with random potentials, showing that the interacting fermion system does not exhibit the full MBL up to very strong disorder, $W \leqslant 20$. Several indicators are inconsistent with accepted requirements for the MBL: (a) spin imbalance correlations $S(t)$ decay to zero as in ergodic systems; (b) local spin correlations $S_l(t)$ decay to zero as well, although with a slow power-law decay; (c) dynamical spin and charge conductivity behaves differently, i.e., we find finite dc value $\sigma_s(0) > 0$, or at least subdiffusive $\sigma_s(\omega \to 0)$, for disorder strengths much above those for which $\sigma_c(0)$ vanishes; and (d) the entanglement entropy $S_2(t)$ does not saturate or increase logarithmically with t, but rather grows according to power law. While the above findings rule out the existence of the full MBL in the model considered, they offer a phenomenon which may be interpreted as a disorder induced dynamical charge-spin separation at all energy scales. It should be pointed out that in a 1D disordered Hubbard model an effective charge-spin separation appears already at weak to modest $U \sim t_0$, which should be distinguished from the $U \gg t_0$ limiting behaviors well known in a pure model [46] and recently reported also for a disordered model [39,47]. We cannot, however, exclude the possibility that charge also would become ergodic at some very long time scale, which is so far beyond numerical as well as experimental reach.

One might speculate that a particular absence of full MBL can be related to SU(2) symmetry [9,48,49] of the Hubbard model. Yet, the non-Abelian SU(2) spin rotation symmetry can be lifted by introducing a constant-magnetic-field term $H' = B \sum_j m_j$, not changing our conclusions. Namely, time evolution of any state with a fixed number of up and down fermions remains the same. Therefore the presence or the absence of SU(2) symmetry is irrelevant for $T \to \infty$ averages (where all states have an equal weight) or for time evolution of specific states from any invariant subspace. It is also evident from our results that the above effective decoupling of charge and spin can be broken by, e.g., an addition of random local (magnetic) fields. If fermions with different spin orientations exhibit independent disorder charge and spin can be both nonergodic and one can have (full) MBL. There is also an interesting possibility that, if we use a spin disorder, i.e., $\sum_j \varepsilon_j (n_{j\uparrow} - n_{j\downarrow})$ instead of the charge disorder, the spin would be localized and the charge delocalized. Therefore, by a simple choice of disorder type we can tune transport properties of spin and charge—a potentially useful property for engineered quantum devices.

Our findings are not in disagreement with measurements of charge degree of freedom in cold-atom experiments, which simulate a quarter-filled 1D Hubbard model and reveal a nonergodic charge imbalance at strong quasiperiodic potential. We show in the Supplemental Material [41] that with a random potential of similar strength the charge is nonergodic, whereas spin correlations decay to zero, exhibiting no localization.

Acknowledgments. P.P. acknowledges fruitful discussions with F. Pollmann and F. Heidrich-Meisner. P.P. and M.Ž. acknowledge the support by the program P1-0044 and Grant No. J1-7279 of the Slovenian Research Agency. O.S.B. acknowledges the support by the Croatian QuantiXLie Center of Excellence.

[1] L. Fleishman and P. W. Anderson, Phys. Rev. B **21**, 2366 (1980).
[2] D. Basko, I. Aleiner, and B. Altshuler, Ann. Phys. (NY) **321**, 1126 (2006).
[3] P. W. Anderson, Phys. Rev. **109**, 1492 (1958).
[4] N. F. Mott, Philos. Mag. **17**, 1259 (1968).
[5] V. Oganesyan and D. A. Huse, Phys. Rev. B **75**, 155111 (2007).
[6] E. J. Torres-Herrera and L. F. Santos, Phys. Rev. B **92**, 014208 (2015).

[7] D. J. Luitz, N. Laflorencie, and F. Alet, Phys. Rev. B **91**, 081103 (2015).
[8] M. Serbyn and J. E. Moore, Phys. Rev. B **93**, 041424(R) (2016).
[9] R. Vasseur, A. J. Friedman, S. A. Parameswaran, and A. C. Potter, Phys. Rev. B **93**, 134207 (2016).
[10] T. C. Berkelbach and D. R. Reichman, Phys. Rev. B **81**, 224429 (2010).
[11] O. S. Barišić and P. Prelovšek, Phys. Rev. B **82**, 161106 (2010).
[12] K. Agarwal, S. Gopalakrishnan, M. Knap, M. Müller, and E. Demler, Phys. Rev. Lett. **114**, 160401 (2015).
[13] S. Gopalakrishnan, M. Müller, V. Khemani, M. Knap, E. Demler, and D. A. Huse, Phys. Rev. B **92**, 104202 (2015).
[14] Y. Bar Lev, G. Cohen, and D. R. Reichman, Phys. Rev. Lett. **114**, 100601 (2015).
[15] R. Steinigeweg, J. Herbrych, F. Pollmann, and W. Brenig, Phys. Rev. B **94**, 180401 (2016).
[16] O. S. Barišić, J. Kokalj, I. Balog, and P. Prelovšek, Phys. Rev. B **94**, 045126 (2016).
[17] M. Žnidarič, A. Scardicchio, and V. K. Varma, Phys. Rev. Lett. **117**, 040601 (2016).
[18] M. Žnidarič, T. Prosen, and P. Prelovšek, Phys. Rev. B **77**, 064426 (2008).
[19] J. H. Bardarson, F. Pollmann, and J. E. Moore, Phys. Rev. Lett. **109**, 017202 (2012).
[20] M. Serbyn, Z. Papić, and D. A. Abanin, Phys. Rev. X **5**, 041047 (2015).
[21] D. A. Huse, R. Nandkishore, and V. Oganesyan, Phys. Rev. B **90**, 174202 (2014).
[22] M. Serbyn, Z. Papić, and D. A. Abanin, Phys. Rev. Lett. **111**, 127201 (2013).
[23] V. Ros, M. Müller, and A. Scardicchio, Nucl. Phys. B **891**, 420 (2015).
[24] J. Z. Imbrie, J. Stat. Phys. **163**, 998 (2016).
[25] C. Monthus and T. Garel, Phys. Rev. B **81**, 134202 (2010).
[26] A. Pal and D. A. Huse, Phys. Rev. B **82**, 174411 (2010).
[27] D. J. Luitz, N. Laflorencie, and F. Alet, Phys. Rev. B **93**, 060201(R) (2016).
[28] M. Mierzejewski, J. Herbrych, and P. Prelovšek, arXiv:1607.04992.
[29] P. Prelovšek and J. Herbrych, arXiv:1609.05450.
[30] D. A. Huse, R. Nandkishore, V. Oganesyan, A. Pal, and S. L. Sondhi, Phys. Rev. B **88**, 014206 (2013).
[31] A. Chandran, V. Khemani, C. R. Laumann, and S. L. Sondhi, Phys. Rev. B **89**, 144201 (2014).
[32] R. Nandkishore and D. A. Huse, Annu. Rev. Condens. Matter Phys. **6**, 15 (2015).
[33] E. Altman and R. Vosk, Annu. Rev. Condens. Matter Phys. **6**, 383 (2015).
[34] M. Schreiber, S. S. Hodgman, P. Bordia, H. P. Lüschen, M. H. Fischer, R. Vosk, E. Altman, U. Schneider, and I. Bloch, Science **349**, 842 (2015).
[35] S. S. Kondov, W. R. McGehee, W. Xu, and B. DeMarco, Phys. Rev. Lett. **114**, 083002 (2015).
[36] P. Bordia, H. P. Lüschen, S. S. Hodgman, M. Schreiber, I. Bloch, and U. Schneider, Phys. Rev. Lett. **116**, 140401 (2016).
[37] J.-Y. Choi, S. Hild, J. Zeiher, P. Schauß, A. Rubio-Abadal, T. Yefsah, V. Khemani, D. A. Huse, I. Bloch, and C. Gross, Science **352**, 1547 (2016).
[38] J. Smith, A. Lee, P. Richerme, B. Neyenhuis, P. W. Hess, P. Hauke, M. Heyl, D. A. Huse, and C. Monroe, Nat. Phys. **12**, 907 (2016).
[39] R. Mondaini and M. Rigol, Phys. Rev. A **92**, 041601(R) (2015).
[40] Y. Bar Lev and D. R. Reichman, Europhys. Lett. **113**, 46001 (2016).
[41] See Supplemental Material at http://link.aps.org/supplemental/10.1103/PhysRevB.94.241104, which includes Refs. [34,36,39,50,51], for data for different L, quarter-filling initial states, Aubry-Andre quasiperiodic disorder, and demonstration of global spin relaxation.
[42] M. W. Long, P. Prelovšek, S. El Shawish, J. Karadamoglou, and X. Zotos, Phys. Rev. B **68**, 235106 (2003).
[43] P. Prelovšek and J. Bonča, *Strongly Correlated Systems—Numerical Methods*, Springer Series in Solid-State Sciences (Springer-Verlag, Berlin/Heidelberg, 2013).
[44] A. Karahalios, A. Metavitsiadis, X. Zotos, A. Gorczyca, and P. Prelovšek, Phys. Rev. B **79**, 024425 (2009).
[45] K. Agarwal, E. Demler, and I. Martin, Phys. Rev. B **92**, 184203 (2015).
[46] M. Ogata and H. Shiba, Phys. Rev. B **41**, 2326 (1990).
[47] S. A. Parameswaran and S. Gopalakrishnan, arXiv:1603.08933.
[48] R. Vasseur, A. C. Potter, and S. A. Parameswaran, Phys. Rev. Lett. **114**, 217201 (2015).
[49] A. C. Potter and R. Vasseur, arXiv:1605.03601.
[50] B. S. Shastry, Phys. Rev. Lett. **56**, 1529 (1986); T. Prosen and M. Žnidarič, Phys. Rev. B **86**, 125118 (2012).
[51] M. Žnidarič, Phys. Rev. Lett. **110**, 070602 (2013).